CrossMark

The distribution of fluids in irregular capillary tubes: a new capillary model based on the single-corner capillary

Long Long[1] · Bing Zhang[1]

Abstract A new basic single-corner capillary model is presented. In this model, the distribution of immiscible fluids is determined by a particular threshold pressure. Additionally, we derive and analyze the interface curvature and profile of the fluid menisci in different tubes. Various polygonal cross sections are obtained by repeatedly superposing the basic single-corner capillary model. We study the relationship between the number of polygon edges and the distribution of fluids as well as the saturation of the wetting phase in equilateral polygon tubes. Furthermore, for the first time, we discuss the interaction of the corners to reveal the five stages of the fluid interfaces with various corner geometries. The dimensionless interface curvature and the radius of the circle are considered to extend our conclusions to similar cross-sectional capillary tubes of different sizes.

Keywords Single-corner capillary · Distribution · Saturation · Interface · Wetting phase

Introduction

The research of flow in pore level tube models is of great importance in revealing the flow mechanism in porous media. It is well known that the channels in real porous media are not built up as the common cylindrical tubes, and the geometric properties of the pores could be represented better by the capillary with triangular or other polygonal cross sections. When a non-wetting fluid is forced into an irregular polygonal tube, a pressure difference between the immiscible fluids occurs if the wetting fluid remains in the corners. This pressure is a function of the cross-sectional geometry, surface tension, and contact angle. Mayer and Stowe (1965) and Princen (1969a; 1969b; 1970) have developed a method to determine this pressure by considering that the surface free energy inside the channel maintains equilibrium. The method they derived was named the MS-P method. The theory at the core of the MS-P method is the work balance of the non-wetting phase displacement, where the work of a very small distance of the main terminal meniscus equals the change in the surface free energy of the arc menisci; the configuration of menisci in a triangular tube is shown in Fig. 1 (Jia et al. 2007). By utilizing the MS-P method, Mason and Morrow (1991) studied the curvature of the menisci under perfect wetting conditions in irregular triangular tubes. They investigated capillary tubes with different cross sections that may have an equal shape factor, G, which was defined as $G = A/P^2$, where A and P are the area and perimeter of the triangular cross section. The shape factor was a reasonable method and was applied by other researchers. Lago and Araujo (2001) also introduced a modified shape factor, multiplied by 4π, and demonstrated that G would reach its maximum value in a capillary with a circular cross section. Considering the presence of the contact angle in natural flow, Jia et al. (2007) extended the work of Mason and Morrow to the case of two-phase flow with arbitrary contact angles, and they derived the distribution of the interface between the two immiscible fluids, controlled by the entry pressure, in a triangular capillary tube. Nevertheless, 3D images provided by high-resolution microtomography (Arns et al. 2005) prove that the pore structures

✉ Long Long
longlong736353@126.com

1 College of Petroleum Engineering, China University of Petroleum, Qingdao 266580, Shandong, People's Republic of China

Fig. 1 Drainage in a triangular tube: **a** the three-dimensional view of the drainage, **b** the cross section of the drainage and the arc menisci, **c** the vertical section of the drainage and the profile of the main terminal meniscus in corner A

(a)

(b)   (c)
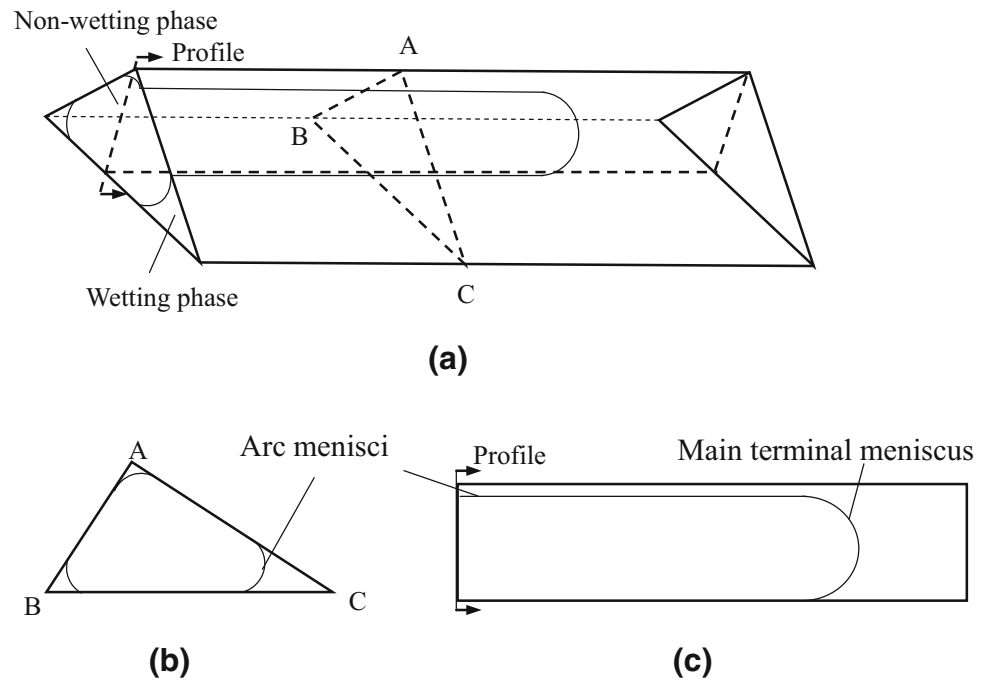
in natural rock are far more complicated than these triangular and rectangular tubes.

Circular, triangular, and rectangular capillary tubes were investigated in previous studies of flow simulation in irregular tubes and pore-scale network modeling (Kovscek et al. 1993; Man and Jing 1999, 2000, 2001). The shape factor of a circular tube is 0.07958, while the shape factors of triangular and rectangular tubes are <0.04811 and 0.06250, respectively. The shape factors reach their maximum values with the equilateral triangle and square cross sections for triangular and rectangular tubes, respectively. This means that the cross sections with shape factors between 0.07958 and 0.06250 are represented by a series of tubes mentioned previously. Irregular triangular tubes with the same shape factor can have geometrically different cross sections (Lago and Araujo 2001; Oren et al. 1998).

In these tubes, when two immiscible fluids flow with the form of piston-like flow, the curvatures of the interfaces are controlled by the capillary pressure; the distributions of the fluids denote their saturations, which have a significant influence on the flow behaviors. Theoretical analysis of the fluid distributions (Jia et al. 2007) indicates that triangular capillary tubes with the same shape factor have slightly different wetting phase saturation profiles. When the contact angle is <50°, the saturations of each fluid in different triangular tubes with the same shape factor are similar, but the difference in the saturations increases slightly with increasing contact angle, after exceeding 50°. Tubes with shape factors between 0.07958 and 0.06250 are more complicated than triangular tubes, and the saturation profiles of the fluids in irregular tubes with the same shape factor are

unknown. Accordingly, it is necessary to study the saturation profiles in tubes with complicated cross sections, and the saturation analysis between the tube bundles with the same shape factor is also a focal point in this research.

Researchers have studied the effect of different contact angles in capillary tubes of fixed geometry to gain a better understanding of the distribution and flow behaviors in regular polygonal tubes. Princen (1969a; 1969b; 1970) has discussed the curvature of menisci in triangular and square tubes with a zero contact angle. Mason and morrow (1984) have shown that with a particular critical contact angle, the wedge menisci would disappear in n-sided polygonal tubes. The critical contact angle would be zero in circular tubes. As n goes to infinity, the n-sided polygonal cross section is similar to a circular cross section. Therefore, Lindquist (2006) indicated that, as the meniscus configuration became coincident with the perimeter of a circle, the radius of the interface was half of the circle radius. In a study by Raeesi et al. (2013), the effect of roughness on the wettability was investigated by using the MS-P theory; the models were tubes with straight grooves along the axial direction on the tube wall, which will be compared with polygonal tubes in this paper.

Following decades of remarkable developments, researchers have aimed to determine the fluid distribution using mathematical models and experimental models (Dong and Chatzis 1995; Dong et al. 1995; Frette and Helland 2010; Jamaloei et al. 2010; Jia et al. 2007; Piri and Blunt 2004; Van Dijke et al. 2004; Van Dijke and Sorbie 2003). With the advent of computed microtomography and the development of image analysis techniques, the

geometrical characterizations and channel cross sections of pores in porous media have become available (Lindquist et al. 1996, 2000; Sholokhova et al. 2009; Wildenschild and Sheppard 2013). This research, on the distribution and flow behaviors of fluids in irregular tubes, can be considered a fundamental study for the residual saturation and flow of fluid in natural rock.

In terms of the flow of fluids in tubes, Ransohoff and Radke (1988) studied the laminar flow of a wetting phase along the corners of a non-circular capillary tube that was originally occupied by a gas phase, and the two-phase flow in their paper was considered to be a two-dimensional hydrodynamic problem that was a function of the cross-sectional geometry, the viscosity, and the contact angle. Unlike in the work of Ransohoff and Radke, in which the two fluids were liquid and gas, the stress between the fluids on the interface is not negligible in the case of liquid–liquid two-phase flow. Additionally, in a liquid–liquid system, the velocity coupling on the interface caused by the interactions between fluids also considerably influences the flow. Other researchers also studied the velocity coupling between the liquids at different viscosities (Patzek and Kristensen 2001). Furthermore, in porous media, the interactions are generally presented as a function of the relative permeability that depends on the saturations of the two phases (Bartley and Ruth 1999).

In this paper, a new basic single-corner capillary model is presented, which is similar to the kite-shaped pore model (Mason and Morrow 1984). The distribution of immiscible fluids is controlled by a particular threshold pressure, meaning that the meniscus curvature of the fluids can be analytically derived with the MS-P method. By repeatedly superposing the basic single-corner capillary model, various polygons are obtained, and the profile of the interfaces within these polygonal tubes is discussed. Admittedly, as the most commonly used research model, the triangular cross-sectional capillary is one of the polygons discussed here. Additionally, the influence of the number of edges of the polygons on the saturation of the wetting fluid in the equilateral polygon tubes, the interaction between the corners, and the saturation difference between the bundle and the polygonal tube with the same shape factor are analyzed in detail. To extend the fluid distribution result to the flow behaviors of fluids and to investigate the application of the tube models in porous media, the results of numerical simulations of the two-phase flow with varying corner combinations, contact angles, and viscosity systems are discussed.

Single-corner capillary model

In the process of non-wetting phase piston-like displacement in a capillary tube, the work balance between a very small displacement of the main terminal meniscus (MTM) and the change in the surface free energy of the arc menisci (AM) controls the distribution of the fixed fluids. The curvatures of the main terminal meniscus and the arc menisci are controlled by the capillary pressure, P_c, and the pressure maintaining the piston-like displacement can be expressed as a function of the cross section geometry and the surface tension:

$$P_c = \frac{(\sigma_{ns} - \sigma_{ws})L_{ns} + \sigma_{nw}L_{nw}}{A_n} \tag{1}$$

where σ, L, and A are the surface tension, length, and area, respectively, and the superscripts n, w, and s refer to the non-wetting phase, wetting phase, and solid phase, respectively. By introducing the Young equation:

$$\sigma_{ns} - \sigma_{ws} = \sigma_{nw} \cos \theta \tag{2}$$

where θ is the contact angle, the P_c function can be simplified to:

$$P_c = \frac{\sigma_{nw}L_{ns} \cos \theta + \sigma_{nw}L_{nw}}{A_n}. \tag{3}$$

When the capillary pressure in the tube reaches equilibrium, the curvatures of the main terminal meniscus and the arc menisci are equal, and the relationship between the capillary pressure and the meniscus radius, R_{-m}, is related to the surface tension:

$$P_c = \frac{\sigma_{nw}}{R_m}. \tag{4}$$

To determine the geometric configuration of the interface between the immiscible fluids, Eqs. (3) and (4) are combined to determine the value of R_{-m}:

$$R_m = \frac{A_n}{L_{ns} \cos \theta + L_{nw}}. \tag{5}$$

As written, Eq. (5) can be applied to calculate the meniscus curvature of the piston-like displacement in a capillary tube with an irregular cross section, including a circle, triangle, and square. To simplify this equation, the numerator and the denominator can be defined as the effective area, A_{eff}, and the effective perimeter, P_{eff}, respectively, which are essential to determine the fluid distributions. In addition, the universal formula of R_m is expressed as (Jia et al. 2007)

$$R_m = \frac{A_{eff}}{P_{eff}}. \tag{6}$$

Equation (6) reflects the core theory of the MS-P method that the work generated by the small displacement of the MTM is equal to the change in the surface free energy of the AM; the complicated analysis in the MS-P method is based on a series of trigonometric derivations, but it is simplified here to solve the problem of menisci in irregular cross-sectional tubes.

Compared to triangular and rectangular capillary tubes, irregular tubes with a polygonal cross section have more corners, such as a pentagon, hexagon, or more complex geometry. Moreover, in irregular tubes, the rough edges of the cross section can be more complicated than the simple convex polygons for the concave portions, which are more similar to the natural pore structures in porous media. For the purpose of determining the fluid distributions in the irregular polygonal capillary tubes, a capillary tube with a single-angle cross section is proposed. Through repeated superpositioning, multiple single-corner capillary models can be combined into a polygonal tube model with a more complex cross-sectional structure.

When the contact angle is equal to 0

The cross section of this new capillary model based on the single-corner capillary is the combination of a circle of radius, R, and a corner with an acute angle, α, $< \pi$, whose corner is shown in Fig. 2. The two edges of the corner, AB and AC, are tangent to the circle portion of the cross section at the points B and C. In the case of perfect wetting, the meniscus touches the edges at the points M and N, and the lengths O'M and O'N are the meniscus radius, R_m, while the center of the meniscus, O', is on the straight line between the vertex, A, and the circle center, O. Since M and B are points of tangency, the lines OB and O'M are perpendicular to the corner edge, indicating that the angles $\angle$AOB and $\angle$AO'M are equivalent. Moreover, the basic geometry literature suggests that the single-corner cross section is axisymmetric along the straight line AO, which
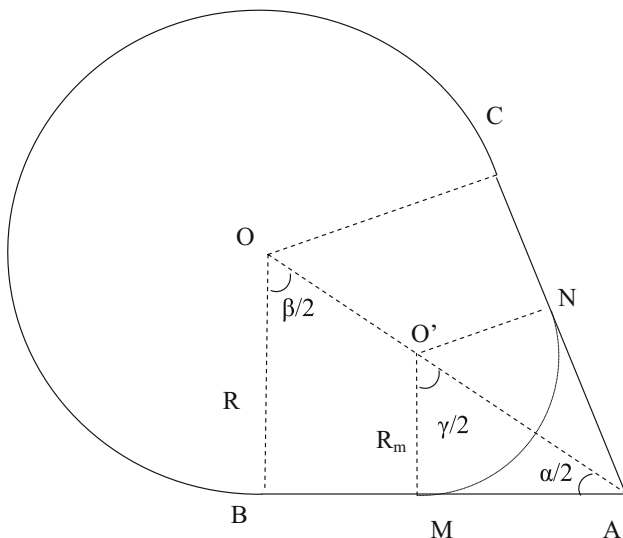

Fig. 2 Cross section of the single-corner capillary tube in the case of complete wetting. The points O and O' are the center of the circle portion of the cross section and the center of the meniscus, respectively

is also the angular bisector to the corner. Therefore, the $\angle$AOB and $\angle$AO'M are the half angles of $\angle$BOC and $\angle$MO'N, symbolized as β and γ, respectively.

In the case of complete wetting, the effective area, A_eff, and the effective perimeter, P_eff, are given, and the formula can be derived from Eq. (6) in terms of AB, AM, and β:

$$R_\mathrm{m} = \frac{\mathrm{AB} \cdot R + \pi R^2 \frac{2\pi - \beta}{2\pi} - \mathrm{AM} \cdot R_\mathrm{m} + \pi R^2 \frac{\beta}{2\pi}}{2\mathrm{AB} + 2\pi R \frac{2\pi - \beta}{2\pi} - 2\mathrm{AM} + 2\pi R \frac{\beta}{2\pi}}. \tag{7}$$

Generally, in the primary geometric relationship, $\alpha + \beta = \pi$, $\mathrm{AB} = R \cot \frac{\alpha}{2}$, and $\mathrm{AM} = R_\mathrm{m} \cot \frac{\alpha}{2}$. By introducing an angle parameter, w, where $w = \cot \frac{\alpha}{2} + \frac{\alpha}{2}$, and simplifying Eq. (7) with the three geometric relationships, the relationship between the meniscus radius and the circle radius can be expressed as:

$$\left(\frac{R_\mathrm{m}}{R}\right)^2 \left(\frac{\pi}{2} - w\right) + \frac{R_\mathrm{m}}{R} \cdot 2\left(\frac{\pi}{2} + w\right) - \left(\frac{\pi}{2} + w\right) = 0. \tag{8}$$

This quadratic equation for the normalized threshold radius, $\frac{R_\mathrm{m}}{R}$, has only one rational solution, which is:

$$\frac{R_\mathrm{m}}{R} = \frac{-(\pi + 2w) + \sqrt{2\pi(\pi + 2w)}}{\pi - 2w}. \tag{9}$$

Equation (9) shows that the normalized threshold radius for a perfect wetting condition is a function of the corner angle, which actually defines the shape of the cross section.

When the contact angle is not equal to 0

Considering the contact angle, θ, in the tube corner, the condition for the presence of the wetting phase is $\theta < \frac{\pi}{2} - \frac{\alpha}{2}$, and the meniscus distribution in this case is shown in Fig. 3. Using the relationships $\alpha + \beta = \pi$, $\alpha + \gamma + 2\theta = \pi$, and $\mathrm{AM} = R_\mathrm{m}\left(\cot \frac{\alpha}{2} \cos \theta - \sin \theta\right)$, the equation of the normalized threshold radius can be written in terms of α and θ:

$$\left(\frac{R_\mathrm{m}}{R}\right)^2 \left[\frac{\pi}{2} - \frac{\alpha}{2} - \theta - \left(\cot \frac{\alpha}{2} \cos \theta - \sin \theta\right) \cos \theta\right] + \frac{R_\mathrm{m}}{R}$$
$$\cdot 2 \cos \theta \left(\frac{\pi}{2} + w\right) - \left(\frac{\pi}{2} + w\right)$$
$$= 0. \tag{10}$$

For a perfect wetting condition, the contact angle is 0, and Eq. (8) is a simplification of Eq. (10). Similar to Eq. (9), the rational solution of this equation is a function of angles, and the relationship between the normalized threshold radius and the contact angle, θ, for different single-corner tube shapes is shown in Fig. 4. The five curves plotted in Fig. 4 represent the normalized threshold radius for tubes with corner angles of 30°, 60°, 90°, 120°, and 150°, which increase with increasing contact angle.
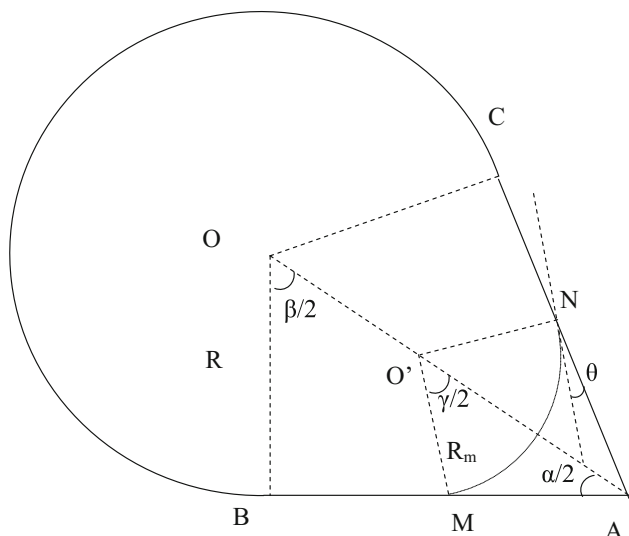
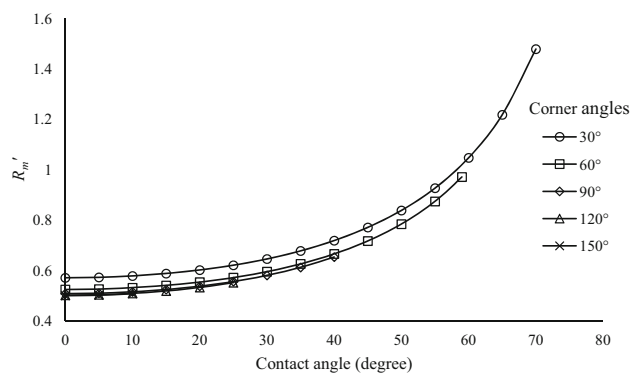**Fig. 3** Cross section of the single-corner capillary with the contact angle, θ

Fig. 4 Normalized threshold radius, $\frac{R_m}{R}$, as a function of the contact angle, θ, and the corner angle, α

The change in the increase gradually increases with larger contact angles. Due to the presence of the wetting phase, the range in the normalized threshold radius for the curves decreases with increasing corner angle. When the contact angle approaches zero, the normalized threshold radius will be a minimum. Additionally, the deceasing intervals between the curves and the phenomenon that the minimum of the normalized threshold radius with the largest corner angle tube is approximately equal to 0.5 illustrate that, as the single corner is smoothed, the meniscus radius is half of the circle radius.

With the single-corner capillary models, the normalized threshold radius of the tubes with complex polygonal cross sections can be calculated by the superposition method. In the next two sections, the tubes with equilateral polygonal cross sections, with corners that can be superposed independently, and more complex tube shapes, with interactional corners, are modeled and discussed in detail.

Equilateral polygon

For an equilateral polygon composed of n vertices and n edges, the corner angle, α, equals $\frac{n-2}{n}\pi$. For a tube with four corners, the effective area and the effective perimeter in Eq. (6) can be expressed as:

$$A_{\text{eff}} = nAB \cdot R + \pi R^2 \frac{2\pi - n\beta}{2\pi} - nAM \cdot R_m \cos\theta + \pi R_m^2 \frac{n\gamma}{2\pi} \tag{11}$$

and

$$P_{\text{eff}} = \left(2nAB + 2\pi R \frac{2\pi - n\beta}{2\pi} - 2nAM \right) \cos\theta + 2\pi R_m \frac{n\gamma}{2\pi}. \tag{12}$$

With the universal formula of R_m, Eq. (6), the solution for $\frac{R_m}{R}$ can be expressed as a function of the contact angle and the number of edges:

$$\frac{R_m}{R} = \frac{-\tan\frac{\pi}{n}\cos\theta + \sqrt{\left(\frac{\pi}{n} - \theta + \sin\theta\cos\theta\right)\tan\frac{\pi}{n}}}{\frac{\pi}{n} - \theta - \left(\tan\frac{\pi}{n}\cos\theta - \sin\theta\right)\cos\theta}. \tag{13}$$

The effect of the contact angle on the normalized threshold radius for different equilateral polygonal tubes with various numbers of edges is plotted in Fig. 5. These equilateral polygons are a regular triangle, quadrilateral, pentagon, hexagon, octagon, and decagon, whose vertices are 60°, 90°, 108°, 120°, 135°, and 144°, respectively. The curves in Fig. 5 have trends similar to the curves in Fig. 4: $\frac{R_m}{R}$ increases with an increasing contact angle, and the ranges of the curves for the tubes with more edges decrease with an increasing number of edges. Moreover, the minimum normalized threshold radius value of the graph also goes to 0.5. This phenomenon indicates that, as n goes to infinity and the cross section is circular, the meniscus profile is coincident with the circumference of the circle and the radius of the meniscus is half the radius of the
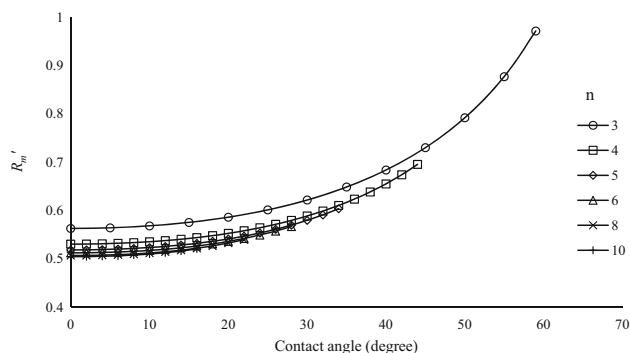

Fig. 5 Normalized threshold radius, $\frac{R_m}{R}$, for different equilateral polygons

circle portion (Lindquist 2006). Therefore, the centers of the menisci constitute a concentric circle of radius $R/2$, and the entry pressure for a cylindrical capillary, $P_c = \frac{2\sigma}{R}$, agrees with the classic literature.

To investigate the smoothing effect on the normalized threshold radius, the relationship of the wetting phase saturation, S, and the number of polygon edges are studied for four different contact angles, 0°, 10°, 20°, and 30°, respectively, using the equation

$$S = \left(\frac{R_m}{R}\right)^2 \left(1 - \frac{\frac{\pi}{n}}{\tan\frac{\pi}{n}}\right),\tag{14}$$

and the result is shown in Fig. 6. The saturation decreases rapidly when the polygon becomes circular, and the decline curve is asymptotic for polygonal cross sections that are more complex than a hexagon. This trend indicates that the proportion of the phase that occupies the tube corners decreases as the corners become more obtuse and the wetting phase saturation is maximized in a triangular capillary tube. At low contact angles, in the same tube, the interface has a greater curvature and a longer length, and the profile of the meniscus in the corner is shown in Fig. 7. It shows that the not-wetting phase is in less contact with the inner walls, and the wetting phase has a greater influ-
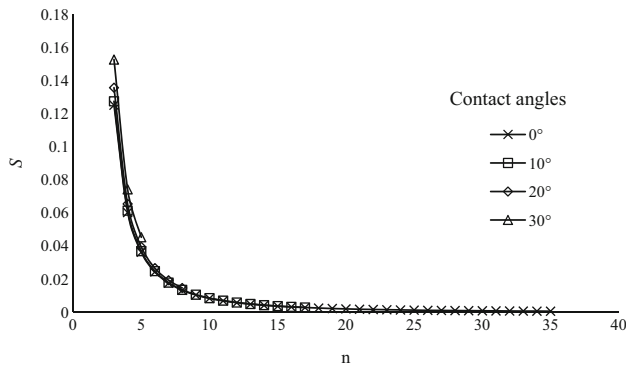

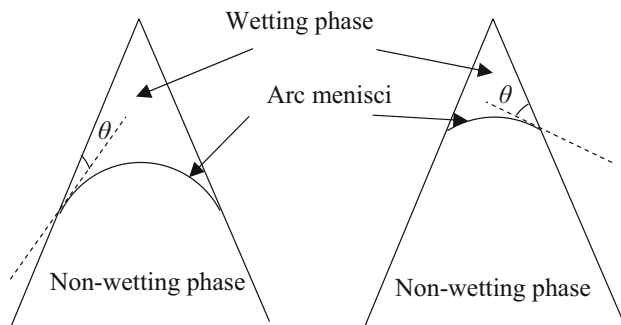**Fig. 6** Wetting phase saturation, S, for different equilateral polygons for four contact angles

Fig. 7 Profile of corner menisci with different contact angles, θ

ence on the flow of the non-wetting phase, when the phase occupying the central region is liquid and does not have a slip effect.

For a polygon with more than 20 edges, the saturation is approximately zero, revealing that the wetting phase behaves as a thin liquid membrane in these cases. When the number of edges goes to infinity, the polygon can be considered circular. Although the film between the non-wetting phase and the inner walls of the tube is extremely thin, the influence of the liquid membrane on two-phase flow is non-negligible, on the condition that the viscosities of the phases are unequal and the scale of the cross section of the tube is very small (Dai et al. 2016; Dai and Wang 2014; Dai and Zhang 2013; Dong et al. 2009; Fairbrother and Stubbs 1935; Taylor 1961). The influence of the film on the flow in the tubes with polygonal cross sections will be discussed in a later section.

Interaction corners

In equilateral polygons, the superposed corners are independent of each other, but they are inscribed in the same circle. However, in natural pores, the cross sections are more irregular, and the complex structure of the polygonal corners forces the fluid distributions to be more complicated.

In a capillary tube with a two-corner cross section, as the corner positions rotate around the center of the circle, the menisci will undergo no change in shape unless the corners start to overlap. The rotating procedure for the two-corner tube model (the corners of $\angle BAC$ and $\angle B'A'C'$, with angle of α) considered here, in which the drainage phase, oil, occupies the central part of the tube, is shown in Fig. 8. When the angle between the bisectors, ψ, is equal to the angle between the lines OB and OC, $\pi - \alpha$, the corners touch along the edge of the cross section, and their tangent points coincide, Fig. 8a (the thick curved lines represent the menisci). Corner intersection occurs when the interfaces are still separated as a consequence of continually decreasing the angle ψ, as illustrated in Fig. 8b and its detail. When the contact angle is constant, the junction of the meniscus and the wall will gradually move away from the vertices of the corners, that is, when the angle ψ decreases to a critical value, the menisci in the two corners will connect, as shown in Fig. 8c. In addition, as the two corners overlap more, the two menisci will merge, as shown in Fig. 8d, and eventually become a single meniscus, as shown in Fig. 8e.

The formula to calculate the threshold radius under different stages of corner overlap was obtained according to the definition of the parameters above. If the corners overlap, the threshold radius can be expressed as:
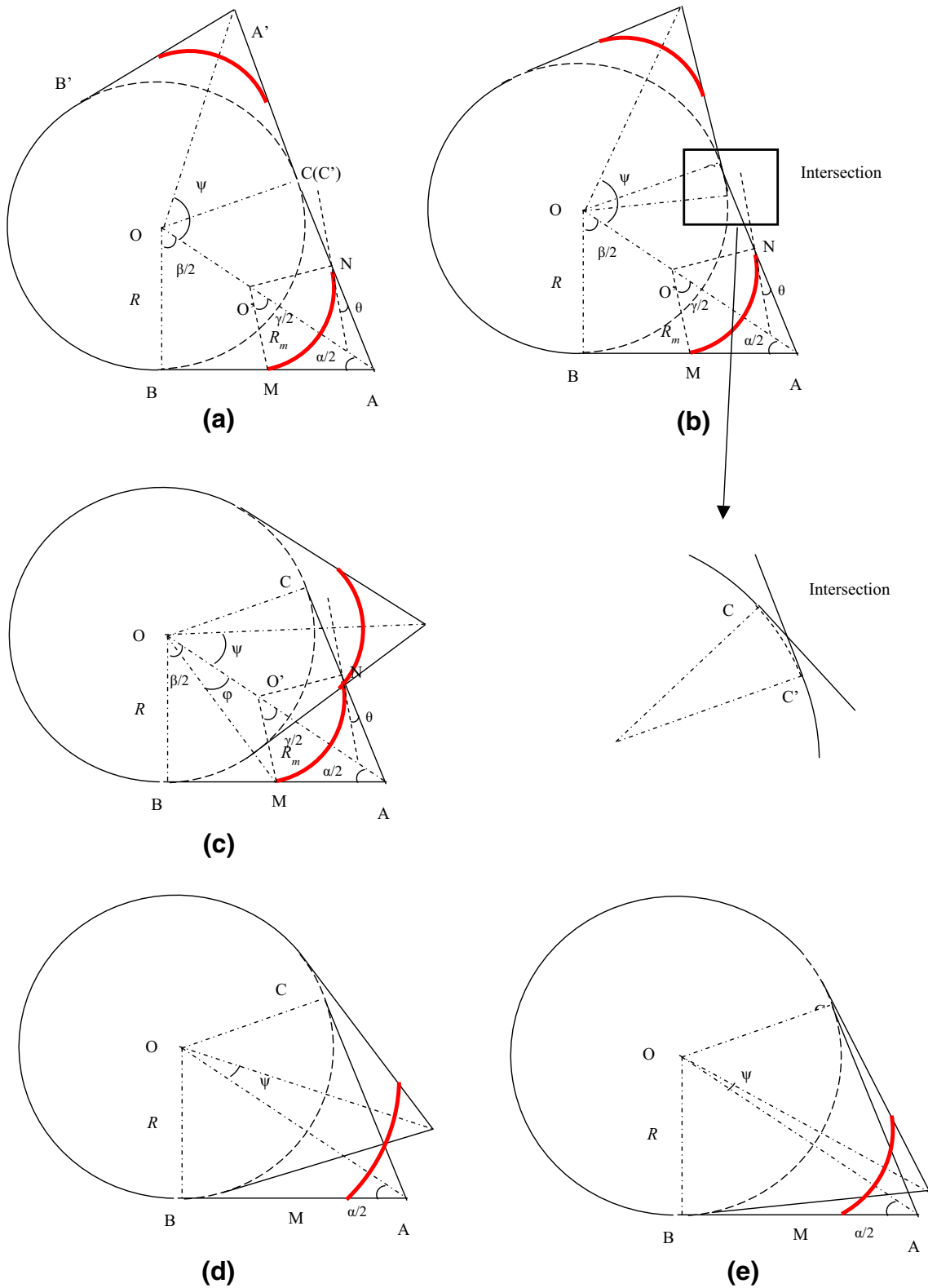
Fig. 8 Profile of various menisci when the two corners are close to each other as they rotate around the center of a circle

$$\left(R_{\mathrm{m}}'\right)^2\left[\pi - \alpha - 2\theta - 2\left(\cot\frac{\alpha}{2}\cos\theta - \sin\theta\right)\cos\theta\right]$$
$$+ R_{\mathrm{m}}'\cos\theta\left[4\cot\frac{\alpha}{2} + 2\alpha - (\pi - \alpha - \psi) - 2\tan\frac{\pi - \alpha - \psi}{2}\right]$$
$$- \left(2\cot\frac{\alpha}{2} + \alpha - \tan\frac{\pi - \alpha - \psi}{2}\right) = 0.$$

(15)

If the two menisci are in contact, the threshold radius can be expressed as:

$$\left(R_{\mathrm{m}}'\right)^2(\pi - \alpha - 2\theta) + R_{\mathrm{m}}'\cos\theta\left(\pi + \alpha - \psi + 2\cot\frac{\alpha}{2}\right)$$
$$- \left(2\cot\frac{\alpha}{2} + \frac{\pi + \alpha - \psi}{2} - \tan\frac{\pi - \alpha - \psi}{2}\right) = 0.$$

(16)

If the meniscus is integrated and separated from the wall, the threshold radius can be expressed as:

$$\left(R_{\mathrm{m}}'\right)^2\left[\frac{\pi - \alpha - 2\theta + \psi}{2} - \cos\theta\left(\cot\frac{\alpha - \psi}{2}\cos\theta - \sin\theta\right)\right]$$
$$+ R_{\mathrm{m}}'\cos\theta\left(\pi + \alpha - \psi + 2\cot\frac{\alpha - \psi}{2}\right)$$
$$- \left[\begin{array}{c}2\cot\frac{\alpha}{2} + \frac{\pi + \alpha - \psi}{2} - \tan\frac{\pi - \alpha - \psi}{2} + \\ \sin\alpha\left(\cot\frac{\alpha}{2} - \tan\frac{\pi - \alpha - \psi}{2}\right)\left(\cot\frac{\alpha - \psi}{2} - \cot\frac{\alpha}{2}\right)\end{array}\right] = 0.$$

(17)

In the case of complete wetting, Fig. 9 shows the relationship between the normalized threshold radius and the angle of the bisectors for various tubes with two corner angles of 30° and 30°, 40° and 40°, 50° and 50°, and 60° and 60°. Similar to the results of the single-corner tube models, as shown in Fig. 4, the tubes with sharper corners have a greater threshold radius.

As shown in Fig. 9, as the angle ψ continues to decrease, the dimensionless meniscus radius increases at
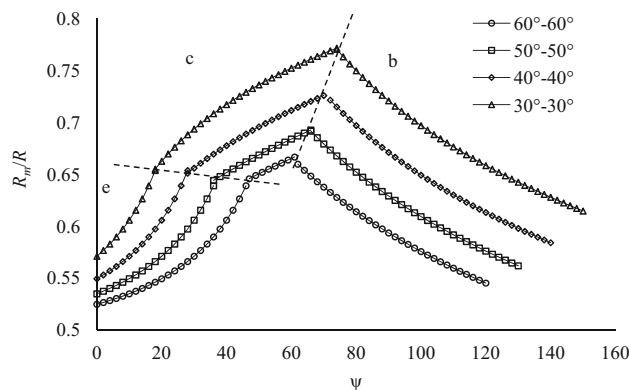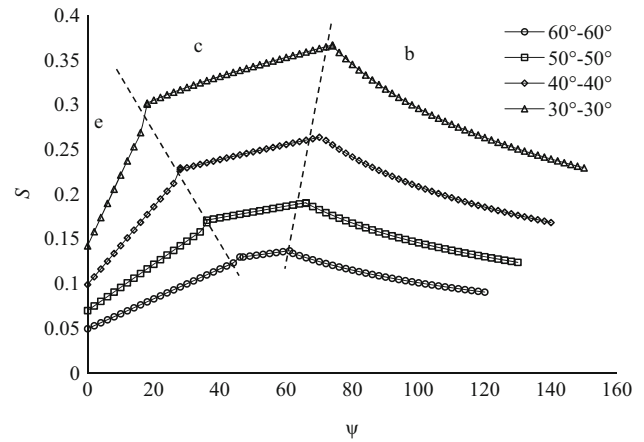

Fig. 10 Wetting phase saturation, S, for different angles between the bisectors

first and then decreases. The results can be divided into three stages, namely b, c, and e, in Fig. 8, and the dashed lines indicate the critical conditions between the different stages. In stage b, R_{m}' increases with decreasing ψ; in stage c, the menisci are in contact with each other, and R_{m}' decreases with decreasing ψ; in stage e, the menisci mix together and separate from the wall, and the change in the decrease in R_{m}' decreases with decreasing ψ and finally reaches the R_{m}' corresponding to the case of a single corner with an equivalent angle.

The saturation of the wetting phase can then be obtained, as shown in Fig. 10. Similar to the curve of the dimensionless radius, with a decrease in the angle ψ, the wetting phase saturation first increases and then decreases. The results show that the wetting phase saturation is higher when the corners of irregular capillary tube are smaller for the same liquid phase system, and the saturation of the wetting phase reaches a maximum value when the two menisci just touch each other.

Conclusions

The single-corner capillary model was presented, and the relationship between the dimensionless radius and the contact angle was studied. The results indicate that with larger contact angles of the same corner capillary tube geometry, the capillary pressure decreases and the meniscus radius becomes larger.

By superposition, the meniscus radius in a capillary tube with a regular polygonal cross section was determined. When the number of edges, n, is <6, the geometry of the cross section has a significant effect on the wetting phase distribution and saturation. As n increases, the wetting phase saturation decreases considerably.

Fig. 9 Normalized threshold radius, $\frac{R_m}{R}$, as a function of the angle, ψ, for different tube shapes

The effects of changing the angle ψ on the meniscus radius and the wetting phase saturation were obtained for three cases. When the corners are in contact with each other, as the angle ψ decreases, the meniscus radius and the wetting phase saturation increase and then decrease and reach a maximum as the two menisci come into contact with each other.

References

Arns CH, Bauget F, Limaye A, Sakellariou A, Senden TJ, Sheppard AP, Sok RM, Pinczewski WV, Bakke S, Berge LI (2005) Pore-scale characterization of carbonates using X-ray microtomography. SPE J 10(4):475–484

Bartley JT, Ruth DW (1999) Relative permeability analysis of tube bundle models. Transp Porous Media 36(2):161–188

Dai L, Wang X (2014) Numerical study on mobilization of oil slugs in capillary model with level set approach. Eng Appl Comput Fluid Mech 8(3):422–434

Dai L, Zhang Y (2013) Experimental study of oil–water two-phase flow in a capillary model. J Pet Sci Eng. 108:96–106

Dai L, Cheng G, Dong M, Zhang Y (2016) The influence of vibratory excitation on the oil slug mobilization in a capillary model. J Pet Sci Res 5(1):1–13

Dong M, Chatzis I (1995) The imbibition and flow of a wetting liquid along the corners of a square capillary tube. J Colloid Interface Sci 172(2):278–288

Dong M, Dullien FA, Chatzis I (1995) Imbibition of oil in film form over water present in edges of capillaries with an angular cross section. J Colloid Interface Sci 172(1):21–36

Dong M, Fan Q, Dai L (2009) An experimental study of mobilization and creeping flow of oil slugs in a water-filled capillary. Transp Porous Media 80(3):455–467

Fairbrother F, Stubbs AE (1935) 119. Studies in electro-endosmosis. Part VI. The "bubble-tube" method of measurement. J Chem Soc 84(5):527–529

Frette O, Helland J (2010) A semi-analytical model for computation of capillary entry pressures and fluid configurations in uniformly-wet pore spaces from 2D rock images. Adv Water Res 33(8):846–866

Jamaloei BY, Kharrat R, Asghari K (2010) Pore-scale events in drainage process through porous media under high-and low-interfacial tension flow conditions. J Pet Sci Eng 75(1):223–233

Jia P, Dong M, Dai L (2007) Threshold pressure in arbitrary triangular tubes using RSG concept for all wetting conditions. Colloids Surf A 302(1–3):88–95

Kovscek A, Wong H, Radke C (1993) A pore-level scenario for the development of mixed wettability in oil reservoirs. AlChE J 39(6):1072–1085

Lago M, Araujo M (2001) Threshold pressure in capillaries with polygonal cross section. J Colloid Interface Sci 243(1):219–226

Lindquist WB (2006) The geometry of primary drainage. J Colloid Interface Sci 296(2):655–668

Lindquist WB, Lee SM, Coker DA, Jones KW, Spanne P (1996) Medial axis analysis of void structure in three-dimensional tomographic images of porous media. J Geo Res Atmos 101(B4):8297–8310

Lindquist WB, Venkatarangan A, Dunsmuir J, Wong TF (2000) Pore and throat size distributions measured from synchrotron X-ray tomographic images of Fontainebleau sandstones. J Geo Res Atmo 105(B9):21509–21527

Man H, Jing X (1999) Network modelling of wettability and pore geometry effects on electrical resistivity and capillary pressure. J Pet Sci Eng 24(2):255–267

Man H, Jing X (2000) Pore network modelling of electrical resistivity and capillary pressure characteristics. Transp Porous Media 41(3):263–285

Man H, Jing X (2001) Network modelling of strong and intermediate wettability on electrical resistivity and capillary pressure. Adv Water Res 24(3):345–363

Mason G, Morrow NR (1984) Meniscus curvatures in capillaries of uniform cross-section. J Chem Soc Faraday Trans 1 Phys Chem Condens Phases 80(9):2375–2393

Mason G, Morrow NR (1991) Capillary behavior of a perfectly wetting liquid in irregular triangular tubes. J Colloid Interface Sci 141(1):262–274

Mayer RP, Stowe RA (1965) Mercury porosimetry—breakthrough pressure for penetration between packed spheres. J Colloid Sci 20(8):893–911

Oren P-E, Bakke S, Arntzen OJ (1998) Extending predictive capabilities to network models. SPE J 3(04):324–336

Patzek T, Kristensen J (2001) Shape factor correlations of hydraulic conductance in noncircular capillaries: II. Two-phase creeping flow. J Colloid Interface Sci 236(2):305–317

Piri M, Blunt MJ (2004) Three-phase threshold capillary pressures in noncircular capillary tubes with different wettabilities including contact angle hysteresis. Phys Rev E 70(6):1–17

Princen HM (1969a) Capillary phenomena in assemblies of parallel cylinders: I. Capillary rise between two cylinders. J Colloid Interface Sci 30(1):69–75

Princen HM (1969b) Capillary phenomena in assemblies of parallel cylinders: II. Capillary rise in systems with more than two cylinders. J Colloid Interface Sci 30(3):359–371

Princen HM (1970) Capillary phenomena in assemblies of parallel cylinders: III. Liquid columns between horizontal parallel cylinders. J Colloid Interface Sci 34(2):171–184

Raeesi B, Morrow NR, Mason G (2013) Effect of surface roughness on wettability and displacement curvature in tubes of uniform cross-section. Colloids Surf A 436:392–401

Ransohoff TC, Radke CJ (1988) Laminar flow of a wetting liquid along the corners of a predominantly gas-occupied noncircular pore. J Colloid Interface Sci 121(2):392–401

Sholokhova Y, Kim D, Lindquist WB (2009) Network flow modeling via lattice-Boltzmann based channel conductance. Adv Water Res 32(2):205–212

Taylor G (1961) Deposition of a viscous fluid on the wall of a tube. J Fluid Mech 10(02):161–165

Van Dijke M, Sorbie K (2003) Three-phase capillary entry conditions in pores of noncircular cross-section. J Colloid Interface Sci 260(2):385–397

Van Dijke M, Lago M, Sorbie K, Araujo M (2004) Free energy balance for three fluid phases in a capillary of arbitrarily shaped

cross-section: capillary entry pressures and layers of the intermediate-wetting phase. J Colloid Interface Sci 277(1):184–201

Wildenschild D, Sheppard AP (2013) X-ray imaging and analysis techniques for quantifying pore-scale structure and processes in subsurface porous medium systems. Adv Water Res 51:217–246